

C₂ Oxygenate Synthesis via Fischer–Tropsch Synthesis on Co₂C and Co/Co₂C Interface Catalysts: How To Control the Catalyst Crystal Facet for Optimal Selectivity

Riguang Zhang,^{†,‡} Guangxiang Wen,[†] Hertanto Adidharma,[‡] Armistead G. Russell,[§] Baojun Wang,^{*,†} Maciej Radosz,[‡] and Maohong Fan^{*,‡,§,||}

[†]Key Laboratory of Coal Science and Technology of Ministry of Education and Shanxi Province, Taiyuan University of Technology, Taiyuan 030024, Shanxi, People's Republic of China

[‡]Department of Chemical Engineering and Department of Petroleum Engineering, University of Wyoming, Laramie, Wyoming 82071, United States

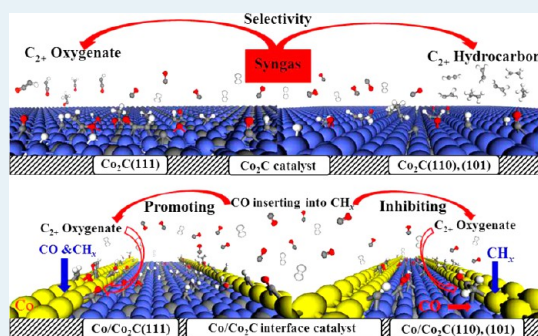
[§]School of Civil and Environmental Engineering, Georgia Institute of Technology, Atlanta, Georgia 30332, United States

^{||}School of Energy Resources, University of Wyoming, Laramie, Wyoming 82071, United States

Supporting Information

ABSTRACT: Density functional theory (DFT) analysis is used to shed light on the intricate effects of the Co₂C and Co/Co₂C catalyst crystal facets on the selectivity of the C₂ oxygenate and hydrocarbon formation in Fischer–Tropsch synthesis. Three representative low-index Co₂C (101), (110), and (111) surfaces, varying in surface energy from low and medium to high, are model examples of different Co₂C exposed crystal facets. Since CH_x ($x = 1–3$), CO, and H species are the key intermediates critical to the C₂ oxygenate selectivity, all Fischer–Tropsch reactions related to CH_x ($x = 1–3$) species, including CO insertion into CH_x ($x = 1–3$) and CH_x + CH_y ($y = 1–3$) coupling to form C₂ species (C₂H_x and C₂H_xO), as well as the hydrogenation and dissociation of CH_x ($x = 1–3$) to form C₁ species (CH₄ and C), are used as examples examined at a typical FTS temperature of 493 K. On Co₂C (101) and (110) surfaces, CH and CH₂ species are dominant form of the CH_x species, CH self-coupling to C₂H₂ and CH coupling with CH₂ to CH₂CH is dominant C₂ species. However, on a Co₂C (111) surface, only CH monomer is a dominant CH_x ($x = 1–3$) species, and CO insertion into CH to form CHCO is a dominant C₂ species. CH₄ and C production on these three surfaces is impossible. These results show that C₂ species formation, rather than C₁ species, is a preferable pathway on different Co₂C crystal facets in FTS reactions. Moreover, the C₂ selectivity, quantitatively estimated from the effective barrier difference, is found to be sensitive to the Co₂C crystal facet. The Co/Co₂C (111) interface catalyst is more favorable for C₂ oxygenate formation in comparison to the pure Co₂C (111) catalyst, whereas the Co/Co₂C (110) and Co/Co₂C (101) interface catalysts are unfavorable for C₂ oxygenate formation in comparison to the pure Co₂C (110) and (101) catalysts. Therefore, for the FTS over Co₂C and Co/Co₂C catalysts, the Co₂C (111) crystal facet is found to have an unexpectedly high selectivity for C₂ oxygenates, whereas the Co₂C (101) and (110) crystal facets are found to have a high selectivity toward C₂ hydrocarbons. The results mean that controlling the crystal facets of Co₂C catalysts using well-defined preparation methods can be an effective tool to tune the FTS selectivity toward the most desirable products.

KEYWORDS: Co₂C, Fischer–Tropsch synthesis, crystal facet, selectivity, density functional theory



1. INTRODUCTION

Fischer–Tropsch synthesis (FTS) converts syngas (CO and H₂) into C₂₊ species¹ over transition metals, such as Co,^{2,3} Fe,⁴ Ru,⁵ Rh,⁶ and Ni.⁷ Among them, Co is known to be relatively more active and more resistant to deactivation on an industrial scale.⁸ However, Co catalysts in the metallic state can form cobalt carbide (Co₂C) under FTS conditions in experiment.^{9,10}

Co₂C formation is known to be a sign of the catalyst deactivation or nonactive species in FTS.^{11–14} However, Volkova et al.¹⁵ proposed Co₂C as being able to activate CO nondissociatively and insert CO into carbonaceous species to

form higher alcohols in FTS at around 500 K. Moreover, the experiments by Xiang and Kruse¹⁶ showed that long-chain *n*-aldehydes and 1-alcohols can be formed over K-promoted CoMn catalysts in FTS reaction from syngas, which contribute to a synergistic interaction between a Mn₃O₈ oxide and a bulk Co₂C phase, and the Co₂C (111) crystal facet is identified by HAADF-STEM images. Other experimental studies^{10,17–21} also

Received: August 17, 2017

Revised: October 19, 2017

Published: October 27, 2017

confirmed that Co_2C plays a significant role in the selectivity for higher alcohol synthesis via FTS from syngas. In contrast, the experiments by Zhong et al.^{22,23} indicated that Co_2C with preferentially exposed Co_2C (101) and (020) crystal facets favor lower olefin production and inhibit CH_4 formation in the FTS reaction. The above studies present two different views of the Co_2C active phase in syngas conversion, one that favors alcohol formation and one that favors lower olefin formation, and suggest an essential difference in the Co_2C crystal facet.

On the other hand, it has to be noted that the formation and stability of bulk Co_2C during the FTS reaction has to get help from the promoters: e.g., La can promote the formation of Co_2C ,^{10,17,18,24} Co_2C quadrangular nanoprisms are formed with the addition of Mn²² or Na,²³ and a bulk Co_2C phase is formed in the presence of K.¹⁶ Moreover, experimental studies^{13,25} have also shown that Co_2C can completely decompose into metal Co when the temperature is higher than 573 K. Actually, when Co_2C catalysts are used for the FTS at typical temperatures of ~ 493 K, the presence of CO in the FTS reaction can significantly stabilize Co_2C , slow down its decomposition, and effectively prevent it from complete decomposition.^{9,13,25} Pei et al.²⁵ experimentally confirmed that Co_2C only partially decomposed into the metal Co at a typical FTS reaction temperature of ~ 493 K. The XRD reveals the presence of the Co_2C phase at 523 K, and XANES and EXAFS results indicate that only a fraction of Co_2C was reduced to metal Co.²⁶ Therefore, Co_2C is the catalyst bulk form under typical FTS conditions. Further, since the metal Co comes from Co_2C decomposition, naturally, a considerable interface between Co and Co_2C is formed, as observed in the HRTEM image, and the Co/ Co_2C interface is the active center for the alcohol synthesis.^{21,25} HRTEM and XRD characterizations by Du et al.²¹ also indicated that the synergistic effect of the metal Co nanoparticles in intimate contact with the Co_2C is responsible for the alcohol synthesis. As mentioned above, both Co_2C and Co/ Co_2C interface catalysts coexist under typical FTS conditions, which lead to two ways to explain active centers in alcohol synthesis, one that Co_2C is the active center and the other that the interface between Co and Co_2C is the active center.

On the basis of the above analysis, since a single-component Co_2C cannot completely exist under the typical FTS conditions, the role of Co_2C crystal facets still remains unclear. The first challenge therefore is to understand the role of single-component Co_2C crystal facets and their effects on product selectivity at a molecular level. Moreover, different Co_2C crystal facets can lead to different Co/ Co_2C interfaces; the second challenge thus is to illustrate the role of different Co/ Co_2C interfaces in alcohol synthesis and their synergistic effects on the alcohol selectivity.

Theoretical calculations have been used as a tool to elucidate the role of the catalyst and the mechanism of typical reactions at a molecular level.^{27–31} Up to now, few theoretical studies have been carried out to understand the roles of a single-component Co_2C catalyst and the Co_2C /Co interface catalysts in synthesis conversion, as well as the effect of Co_2C crystal facets on higher alcohol synthesis from syngas. Li and co-workers^{10,25} did density functional theory (DFT) calculations to understand the nature of different Co_2C crystal facets and the effect of Co_2C crystal facet on CO adsorption and activation, and DFT studies by Zhong et al.²² probed into the formation of lower olefins and methane on different Co_2C crystal facets.

The goal of this study, therefore, is to understand the role of Co_2C and the effect of Co_2C crystal facets on the selectivity of high alcohol synthesis in the FTS reaction from syngas using DFT calculations for a single-component Co_2C to probe the formation of C_2 oxygenates and hydrocarbons, in which C_2 oxygenate represents the high alcohols. A wide range of reactions, including CO insertion into CH_x ($x = 1–3$) to C_2 oxygenates, CH_x coupling to C_2 hydrocarbons, and the hydrogenation or dissociation of CH_x ($x = 1–3$) to CH_4 or C on different Co_2C model surfaces, are examined. On the other hand, C_2 oxygenate formation on Co/ Co_2C interface catalyst with different Co_2C crystal facets is considered to probe the role of different Co/ Co_2C interfaces, the synergistic effect of Co and Co_2C , and the effect of Co_2C crystal facets on the selectivity of alcohol synthesis. Such results can be applied to guide the design of highly selective Co_2C catalysts toward high alcohol synthesis in the FTS reaction.

2. COMPUTATIONAL MODELS AND METHODS

2.1. Surface Models. Co_2C has an orthorhombic structure with the space group $Pmnm$, as shown in Figure S1 in the Supporting Information. All Co and C atoms are equivalent with two formula units per unit cell. C atoms occupy the octahedral interstitial sites of Co, while C atoms and Co atoms are six-coordinated and three-coordinated, respectively.

Earlier work at the Bureau of Mines using Co/ ThO_2 /Kieselguhr catalysts³² and Weller et al.¹³ showed that the bulk Co_2C is not a catalytically active substrate during the FTS reaction; experiments by Pei et al.²⁰ indicated that the surface Co_2C was responsible for the formation of alcohols, and the bulk Co_2C was inert in the FTS reaction. However, in recent years, the experiments of FTS from syngas over Co_2C catalysts have shown that the lower olefins are easily formed over Co_2C with preferentially exposed Co_2C (101) and (020) crystal facets, as observed by high-resolution HRTEM images and TEM-EDX analyses.^{22,23} Over K-promoted CoMn catalysts in FTS from syngas,¹⁶ the Co_2C (111) crystal facet is identified by HAADF-STEM images. Pei et al.^{9,25} have observed Co_2C (101), (001), (110), (020), and (002) using HRTEM and XRD characterizations in high alcohol synthesis via the FTS reaction at the Co/ Co_2C interface. DFT studies by Zhao et al.¹¹ suggested the stability order of low-index Co_2C surfaces: (101) > (011) > (010) > (110) > (100) > (111).

On the basis of the studies reported above, Co_2C (101), (011), (010), (110), (100), and (111) low-index facets are found to be the dominantly exposed crystal facets with corresponding surface energies of 129, 135, 144, 161, 170, and 170 $\text{meV}/\text{\AA}^2$, respectively. These surfaces correspond to 40.72, 35.21, 11.80, 9.87, 2.08, and 0.27% area proportions of the various exposed Co_2C facets from Wulff construction.

In order to characterize the effect of Co_2C crystal facets on the selectivity of C_2 oxygenates, three representative low-index Co-terminated Co_2C (101), (110), and (111) facets with low, medium, and high surface energies were employed to model different Co_2C crystal facets, in which Co-terminated Co_2C facets represent a typical structure under hydrogen-rich conditions (lower CO/ H_2 ratio) in FTS reactions.⁹

The $p(2 \times 2)$, $p(2 \times 1)$, and $p(2 \times 2)$ supercell slabs were utilized for Co_2C (101), (110), and (111) crystal facets, respectively (Figure 1). A detailed description of these surfaces is presented in Part 1 in the Supporting Information. For Co_2C (101) and (110) facets, the first wrinkle surface only includes Co atoms, and C atoms appear at the second layer only. The

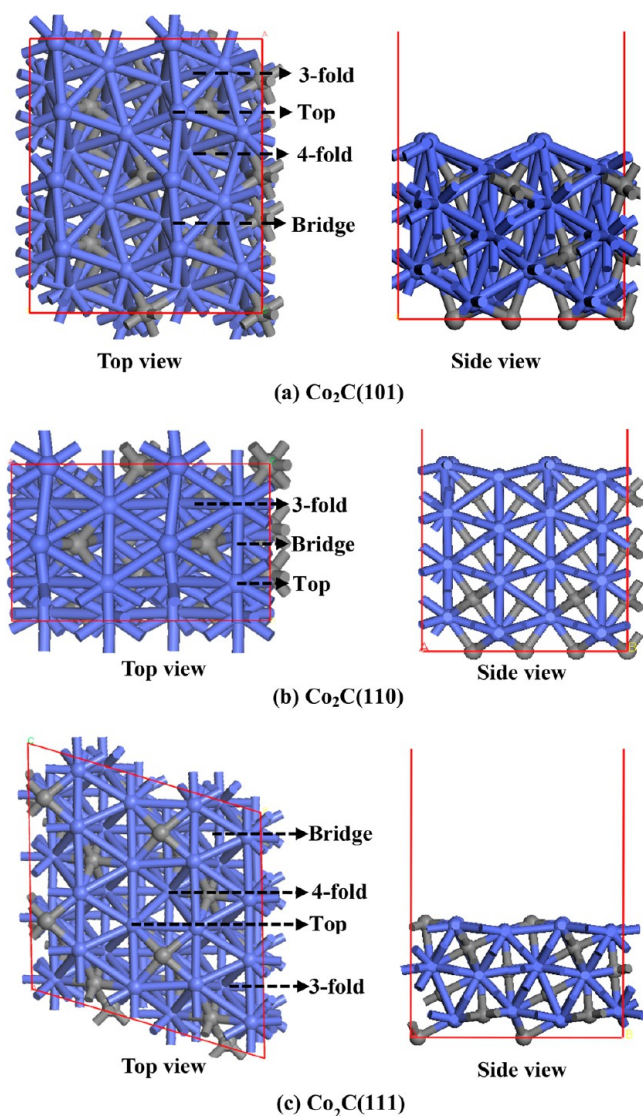


Figure 1. Surface morphology and the corresponding adsorption sites of (a) Co_2C (101), (b) Co_2C (110), and (c) Co_2C (111) surfaces.

Co_2C (111) facet exposes C atoms coordinating with four Co atoms. Thus, since only C atoms exist on the Co_2C (111) facet, the differences among these three facets should contribute to the different characteristics for the adsorption of CH_x , CO, and H atoms, as well as the C–C chain formation on the Co_2C catalyst.^{33,34}

2.2. Computational Methods. Spin-polarized calculations based on density functional theory (DFT), as implemented in the Vienna ab initio Simulation Package (VASP),^{35–37} were performed using the projector augmented wave (PAW)^{38–40} method. The Perdew–Wang 91 (PW91) functional^{41,42} was used. A plane-wave basis set with a cutoff kinetic energy of 400 eV was employed. Monkhorst–Pack⁴³ mesh k -point samplings of $(3 \times 3 \times 1)$, $(4 \times 3 \times 1)$, and $(3 \times 3 \times 1)$ were utilized for the calculations on Co_2C (101), (110), and (111) facets, respectively. The energy and force convergence correspond to 10^{-4} eV and 0.04 eV/Å, respectively. Transition states (TSs) were searched using the climbing image nudged elastic band (CI-NEB) method.^{44,45} The located TSs were optimized using the Dimer method.^{46,47} The vibrational frequencies were calculated to verify the transition states corresponding to only

one imaginary frequency in true TSs (see Table S1 in the Supporting Information). In addition, the effects of functional choice on the calculated results have been tested, as shown in Table S2 in the Supporting Information. The adsorption energies of CO and CH species, as well as the activation energies of CH self-coupling and CO insertion into CH reactions at 0 K using PW91 and PBE functionals, suggest that there is negligible difference between these two functionals. Moreover, this study aims at probing the effect of Co_2C crystal facets on the selectivity of high alcohol synthesis; thus, we need to obtain the preferred reaction among the reactions related to CH_x ($x = 1–3$) species only by the qualitative comparison with the relative values of the free energy barriers instead of the quantitative results with the absolute values of the free energy barriers. Therefore, the PW91 functional was suitable for the system in this study, and the obtained results are reliable.

Given the contributions of zero-point vibrational energy (ZPE), thermal energy, and entropy to the molar Gibbs free energy, the statistical thermodynamics formulas derived from the partition function were used to correct the total energy obtained directly from such DFT calculations. Since the FTS reactions typically proceed at the temperatures of 473–623 K,^{27,48–51} all energies including the adsorption free energy, the free energy barrier, and the reaction free energy were calculated at 493 K.^{9,25} The reaction rate constant (k) was obtained using harmonic transition state theory (TST).^{52,53} A detailed description of calculating the Gibbs free energy for the gaseous and adsorbed species and the reaction rate constants is presented in Part 2 in the Supporting Information.

3. RESULTS AND DISCUSSION

3.1. Key Intermediates Related to C_2 Species Formation. Recent studies by Li and co-workers^{9,25} showed that, considering FTS reaction temperature (493 K), the barriers are too high for CO direct dissociation on Co_2C (101), (110), and (111) surfaces in comparison to CO nondissociative adsorption and hydrogen-assisted CO dissociation to form CH. This means that the Co_2C facets can provide efficient sites for CO nondissociative adsorption and hydrogen-assisted CO dissociation to form CH. Moreover, Liu et al.⁵⁴ suggested that most of the exposed Co facets are active for CO direct dissociation into C, followed by its hydrogenation to CH_x ($x = 1–3$) species. On the other hand, in order to understand what kind of CH_x species primarily participate in C–C chain formation on the Co surface, Ge et al.⁵⁵ found that CH and CH_2 were the most favored CH_x species on the Co (0001) surface, whereas CH species is the most favored,⁵⁰ CH_2 is the most favored species.²⁸ Our DFT studies of FTS⁵⁶ showed that both CH_2 and CH_3 are the abundant CH_x species on the Co (10–10) surface and that the CH is the surface abundant species on the Co (10–11) surface.

On the basis of the above analysis, the contribution to CH_x ($x = 1–3$) species formation would occur on the Co catalyst by CO direct dissociation and on the Co_2C catalyst by hydrogen-assisted CO dissociation, respectively. Then, the CH_x ($x = 1–3$) hydrogenation leads to CH_4 , the coupling of CH_x leads to C_2 hydrocarbons, and CO insertion into CH_x leads to C_2 oxygenates. Considering the uncertainty in CH_x monomer on the Co surface, the C–C chain formation is extended to CH_x ($x = 1–3$) species in this study. In general, CH_x ($x = 1–3$), CO, and H species are the key intermediates related to the elementary steps that are critical to C_2 species selectivity in the

Table 1. Elementary Reactions and the Corresponding Free Energy Barriers (ΔG_a /eV), Reaction Free Energies (ΔG /eV), and Effective Barrier (E_{eff} /eV) at 493 K for CH_x ($x = 1-3$) Species on the Co_2C (101), (110), and (111) Surfaces

reaction	transition state ^a	Co_2C (101)			Co_2C (110)			Co_2C (111)		
		ΔG_a	ΔG	E_{eff}	ΔG_a	ΔG	E_{eff}	ΔG_a	ΔG	E_{eff}
$\text{CH}=\text{C} + \text{H}$	TSn-1	0.53	-0.33	1.02	0.88	0.28	1.09	1.34	-0.17	1.42
$\text{CH} + \text{H}=\text{CH}_2$	TSn-2	0.91	0.81	1.20	0.60	0.36	0.83	0.46	0.32	0.55
$\text{CH} + \text{CH}=\text{C}_2\text{H}_2$	TSn-3	0.37	0.22	0.93	0.89	0.24	1.34	1.22	0.97	1.41
$\text{CH} + \text{CH}_2=\text{CHCH}_2$	TSn-4	1.58	0.57	2.68	0.29	-0.16	0.56	1.48	0.78	2.57
$\text{CH} + \text{CH}_3=\text{CHCH}_3$	TSn-5	1.08	0.48	2.30	0.99	0.14	1.52	0.81	0.05	2.60
$\text{CH}_2=\text{CH} + \text{H}$	TSn-7	0.10	-0.81	0.73	0.24	-0.36	0.27	0.14	-0.32	1.15
$\text{CH}_2 + \text{H}=\text{CH}_3$	TSn-8	0.44	0.07	1.09	0.61	0.28	0.65	0.94	0.58	1.96
$\text{CH}_2 + \text{CH}_2=\text{C}_2\text{H}_4$	TSn-9	0.73	-0.25	2.09	0.50	0.10	0.53	1.66	0.56	3.65
$\text{CH}_2 + \text{CH}_3=\text{CH}_2\text{CH}_3$	TSn-10	0.90	0.12	2.38	1.56	0.43	1.87	1.92	0.61	4.63
$\text{CH}_3=\text{CH}_2 + \text{H}$	TSn-12	0.37	-0.07	1.08	0.33	-0.28	1.27	0.36	-0.58	2.00
$\text{CH}_3 + \text{H}=\text{CH}_4$	TSn-13	0.69	0.15	1.54	0.96	0.25	0.37	0.61	-0.08	2.28
$\text{CH}_3 + \text{CH}_3=\text{C}_2\text{H}_6$	TSn-14	1.36	0.08	2.91	2.92	0.30	3.49	1.67	-0.35	5.11
$\text{CH} + \text{CO}=\text{CHCO}$	TSn-6	0.93	0.79	1.20	1.19	1.04	1.38	0.97	0.59	1.08
$\text{CH}_2 + \text{CO}=\text{CH}_2\text{CO}$	TSn-11	0.99	0.71	1.66	1.60	1.05	1.65	1.19	1.05	2.22
$\text{CH}_3 + \text{CO}=\text{CH}_3\text{CO}$	TSn-15	1.18	0.75	2.00	1.55	1.14	1.76	1.28	0.48	2.87

^a $n = 1-3$ represent the transition states on Co_2C (101), (110), and (111) surfaces, respectively.

FTS reaction: i.e., CO insertion into CH_x to C_2 oxygenates and $\text{CH}_x + \text{CH}_y$ ($x, y = 1-3$) coupling to C_2 hydrocarbons.

Thus, this study focuses on the reactions to form C_2 species, including the C-C chain formation by CO insertion into CH_x ($x = 1-3$) and the $\text{CH}_x + \text{CH}_y$ ($x, y = 1-3$) coupling to form C_2 species (C_2H_x and $\text{C}_2\text{H}_x\text{O}$) on Co_2C (101), (110), and (111) surfaces. Meanwhile, the hydrogenation and dissociation of CH_x ($x = 1-3$) to form C_1 species (CH_4 and C) is also examined.

The most stable adsorption configurations, the corresponding adsorption free energy, and the key structural parameters of possible species in the process of C_1 and C_2 species formation on the Co_2C (101), (110), and (110) surfaces are presented in Part 3 in the Supporting Information. Meanwhile, the effective barrier of the reactions related to CH_x species (E_{eff} derivation details are given in Part 4 in the Supporting Information) was used as a descriptor to evaluate the reaction rate of the reactions related to CH_x ($x = 1-3$) species, in which the coverage of C_1 species CH_x , CO, and H species as well as the available sites, θ_{CH_x} , θ_{CO} , θ_{H} , and θ_* have been considered. Table 1 gives the free energy barriers, reaction free energies, and effective barriers of all elementary reactions related to CH_x ($x = 1-3$) species over Co_2C (101), (110), and (111) surfaces at 493 K. The rate constants at 443, 468, 493, 518, and 543 K are given in Table S3 in the Supporting Information.

3.2. Reactions Related to CH_x ($x = 1-3$) Species on Co_2C (101). Figures S5-S7 in the Supporting Information present the potential energy profiles of the reactions related to CH_x ($x = 1-3$) species on the Co_2C (101) surface at 493 K together with the corresponding structures. In order to analyze the possible C_1 and C_2 products, starting from the CH_3 species, only the first three favorable reactions related to CH_x ($x = 1-3$) species on Co_2C (101) are presented in Figure 2.

For the CH_3 species, CH_3 dissociation into CH_2 has the lowest free energy barrier of 0.37 eV, which is lower by 0.32 and 0.63 eV in comparison to those for CH_3 hydrogenation to CH_4 (0.69 eV) and CH_3 coupling with CH_2 to CH_3CH_2 (0.90 eV), respectively. Similarly, CH_3 dissociation into CH_2 has the lowest effective barrier. Namely, CH_3 prefers to be dissociated into CH_2 rather than being hydrogenated to CH_4 and being

coupled with CH_2 to CH_3CH_2 . Moreover, only CH_3 dissociation into CH_2 is slightly exothermic (0.07 eV). Thus, CH_3 dissociation into CH_2 is much more favorable both kinetically and thermodynamically among all of the reactions related to the CH_3 species.

For the CH_2 species, CH_2 dissociation into CH has a very low free energy barrier of 0.10 eV, and it is strongly exothermic by 0.81 eV. However, CH_2 self-coupling to C_2H_4 and CO insertion into CH_2 to give CH_2CO have higher free energy barriers of 0.73 and 0.99 eV, respectively, and CO insertion into CH_2 is strongly endothermic (0.71 eV); CH_2 self-coupling to C_2H_4 is exothermic by 0.25 eV, which is far less than the barrier for CH_2 dissociation into CH . Accordingly, CH_2 dissociation into CH has the lowest effective barrier. Thus, the CH_2 species prefers to be dissociated into CH both kinetically and thermodynamically, among all of the reactions related to the CH_2 species.

For the CH species, CH self-coupling to C_2H_2 has the lowest free energy barrier of 0.37 eV, which is lower by 0.16 eV than that for the second favorable reaction of CH dissociation into C. The third is CO insertion into CH to CHCO with a free energy barrier and reaction free energy of 0.93 and 0.79 eV, respectively. Similarly, CH self-coupling to C_2H_2 has the lowest effective barrier. Thus, CH self-coupling to C_2H_2 is more favorable kinetically among all of the reactions related to the CH species.

The above results obtained by the free energy barrier and effective barrier show that, once the CH_3 species appears on the Co_2C (101) surface, it prefers to dissociate into CH_2 , and the CH_2 species further dissociates into CH . Subsequently, the CH species, as the most favored monomer on the Co_2C (101) surface, can easily self-couple to form the dominant C_2 species C_2H_2 . Further, the formation of CH_4 and C is unlikely to occur due to the relatively higher free energy barrier and effective barrier on the Co_2C (101) surface.

Thus, the Co_2C (101) surface exhibits a high catalytic activity and selectivity toward the formation of C_2 hydrocarbon C_2H_2 rather than C_2 oxygenates. These calculated results agree with previous experimental results²² and confirm that the preferentially exposed Co_2C (101) surface favors increased production of lower olefins and inhibits CH_4 formation. As shown in

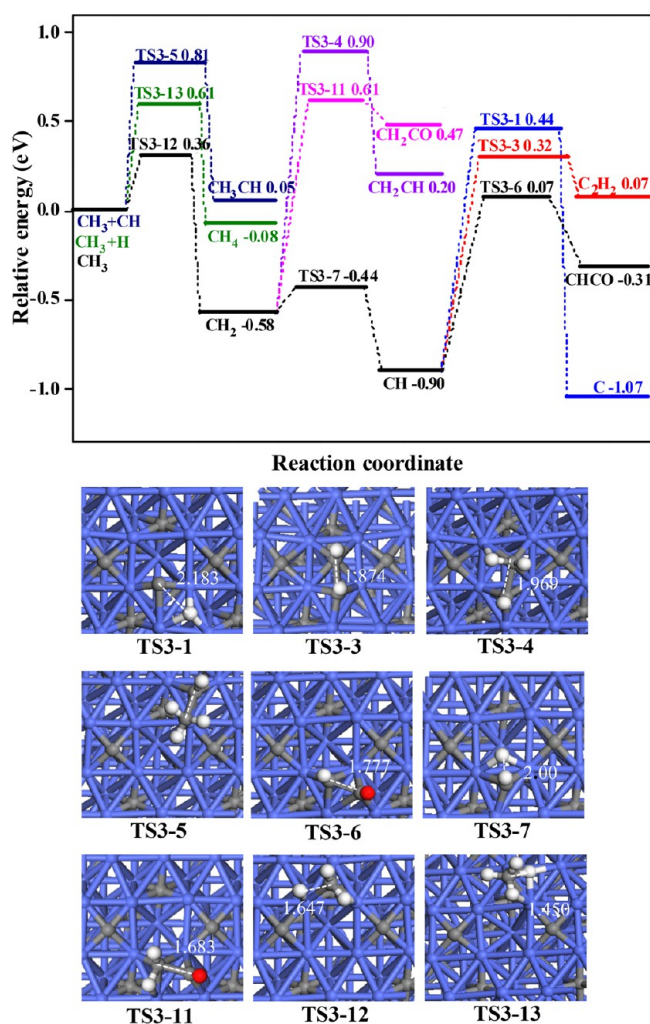


Figure 4. Potential energy profile of Gibbs free energy (493 K) for the first three favorable reactions related to CH_x ($x = 1-3$) species together with transition states (TSs) starting from CH₃ species on the Co₂C (111) surface. The structures of initial states (ISs) and final states (FSs) are shown in Figures S4 and S11–S13 in the Supporting Information.

reactions related to CH species. Finally, the results drawn by the effective barrier agree with those by the free energy barrier.

On the basis of above analysis, once both CH₃ and CH₂ species appear on the Co₂C (111) surface, they will kinetically and thermodynamically prefer to be dissociated into CH rather than be engaged in other reactions, suggesting that only CH monomer is an abundant CH_x ($x = 1-3$) species. Moreover, recent DFT studies^{9,22} have fully investigated the stability of adsorbed CO over Co₂C (101), (110), and (111) surfaces, indicating that the Co₂C surfaces can provide efficient sites for CO nondissociative adsorption and hydrogen-assisted CO dissociation rather than CO direct dissociation; meanwhile, the experimental studies by Volkova et al.¹⁵ have confirmed Co₂C as being able to activate CO nondissociatively. Thus, CO is the abundant surface species in syngas conversion over the Co₂C surface. As a result, CO insertion into CH to form CHCO would be the dominant C₂ species on the Co₂C (111) surface, in contrast to the case for the Co₂C (101) and (110) surfaces. Meanwhile, both CH₄ and C formation would still be difficult due to the high free energy barriers and the effective barriers. Thus, the Co₂C (111) surface exhibits a high catalytic activity

and selectivity toward the formation of C₂ oxygenates CHCO instead of C₂ hydrocarbons.

3.5. Effect of Crystal Facets on the C–C Chain Formation Mechanism over Co₂C Catalyst. As discussed above, C₂ species, rather than C₁ species, prefer to be formed on the Co₂C (101), (110), and (111) surfaces in FTS reactions: namely, the Co₂C surface favors the C–C chain formation. Figure 5 presents the potential energy profile for the

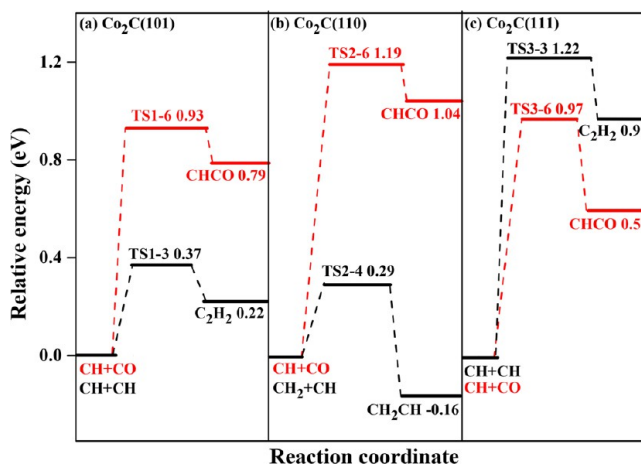


Figure 5. Potential energy profile for the favorable formation pathways related to CH_x coupling to C₂H_y and CO insertion into CH_xCO species on Co₂C (101), (110), and (111) surfaces.

favorable formation pathways related to CH_x coupling to C₂H_y and CO insertion into CH_xCO on the Co₂C (101), (110), and (111) surfaces.

On the Co₂C (101) and (110) surfaces, CH self-coupling to C₂H₂ and CH coupling with CH₂ to CH₂CH intermediate can occur over the Co (0001) and Ru (0001) surfaces in the FTS mechanism.⁵⁵ The theoretical studies by Cheng et al.⁵⁰ showed that CH self-coupling to C₂H₂ is favored on the flat Co (0001) surface. CH self-coupling to C₂H₂ is also the most likely coupling pathway in terms of the carbide mechanism over the terraced-like χ -Fe₅C₂ (510) surface.³⁴ However, on the Co₂C (111) surface, CO insertion into CH to CHCO dominates the C–C chain formation mechanism, which is responsible for C₂ oxygenate formation. For the structural differences among the Co₂C (101), (110), and (111) surfaces, the surface C atoms of Co₂C (111) cause an uneven charge distribution and make the Co atoms attain nonmetallic properties,^{22,30} which is likely to decrease its catalytic activity toward C₂ hydrocarbon formation.

On the other hand, previous studies^{33,34,57} showed that the C–H bond activation of CH_x is primarily guided by the electron back-donation from metal atoms to the antibonding σ -CH* state of CH_x; the C–H bond activation of CH_x is unfavorable for the coupling of CH_x to form C₂ hydrocarbons, and the catalyst surface with the d-band center far from the Fermi energy is more active for CH_x coupling to form C₂ hydrocarbons. According to our projected density of states (PDOS) for the Co₂C (101), (110), and (111) surfaces shown in Figure 6a, the d-band center of the Co₂C (111) surface is closer to the Fermi level with a higher d-band energy of -1.59 eV in comparison to that observed on the Co₂C (101) and (110) surfaces with d-band energies of -1.72 and 1.74 eV,

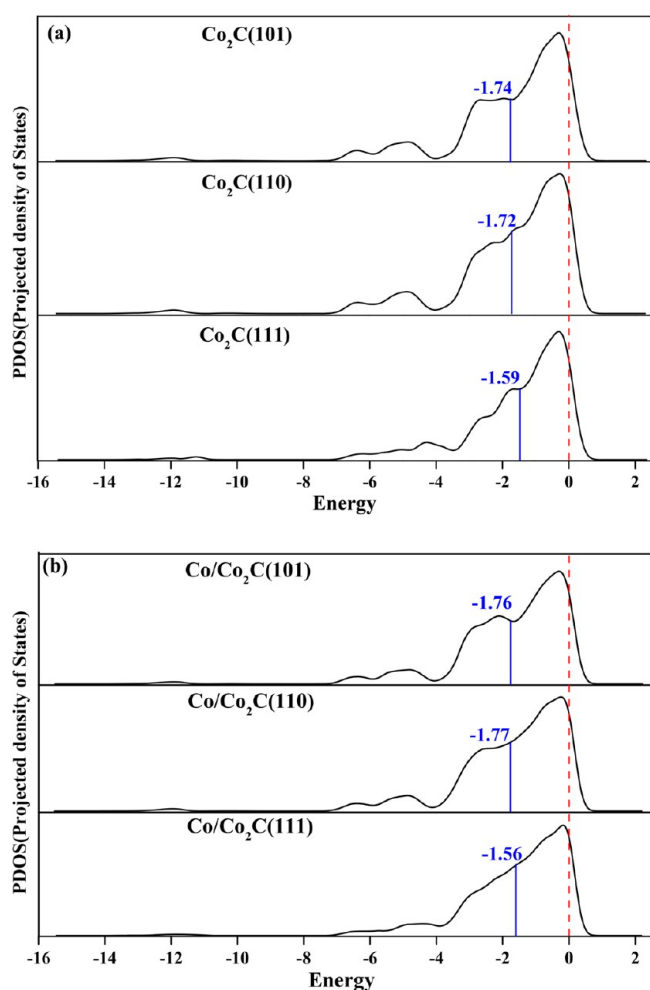


Figure 6. Projected density of states (PDOS) for Co atoms over (a) Co_2C and (b) $\text{Co}/\text{Co}_2\text{C}$ catalysts. The blue solid line indicates the d-band center; the red dotted line denotes the Fermi level.

respectively, suggesting that both Co_2C (101) and (110) surfaces are more active for CH_x coupling to C_2 hydrocarbons in comparison to the Co_2C (111) surface, which agrees with our kinetics results. Therefore, the mechanism of C–C chain formation is highly sensitive to the Co_2C surface structure: namely, the Co_2C crystal facet affects the C–C chain formation mechanism.

3.6. Selectivity between C_2 Oxygenates and Hydrocarbons over Co_2C Catalyst. As mentioned above, the Co_2C (111) surface exhibits a high selectivity toward C_2 oxygenates over C_2 hydrocarbons; however, both Co_2C (101) and (110) surfaces exhibit a high selectivity toward C_2 hydrocarbons. To further quantify the selectivity between C_2 hydrocarbons C_2H_x (CH_2CH and C_2H_2) and C_2 oxygenates $\text{C}_2\text{H}_x\text{O}$ (CHCO) on the Co_2C (101), (110), and (111) surfaces, the effective barrier difference^{50,58–60} between C_2H_x and $\text{C}_2\text{H}_x\text{O}$, ΔE_{eff} has been employed as a descriptor to analyze and evaluate the FTS selectivity over different Co_2C crystal facets, in which the coverage of C_1 species CH_x and CO and H species, as well as the available sites, θ_{CH_x} , θ_{CO} , θ_{H} , and θ_* , have been considered.

As given in Table 2, the values of ΔE_{eff} are -0.27 , -0.82 , and 0.33 eV on Co_2C (101), (110), and (111) surfaces, respectively, suggesting that both Co_2C (101) and (110) surfaces have a higher selectivity toward C_2H_x formation, while the Co_2C (111) surface has a higher selectivity toward $\text{C}_2\text{H}_x\text{O}$ formation.

Table 2. Effective Barrier and Effective Barrier Difference Involved in the Most Favorable Formation Reactions of C_2H_x and $\text{C}_2\text{H}_x\text{O}$ Species on Co_2C (101), (110), and (111) Surfaces^a

surface	$E_{\text{eff,C}_2\text{H}_x}/\text{eV}$	$E_{\text{eff,C}_2\text{H}_x\text{O}}/\text{eV}$	$\Delta E_{\text{eff}}/\text{eV}$
Co_2C (101)	0.93	1.20	-0.27
Co_2C (110)	0.56	1.38	-0.82
Co_2C (111)	1.41	1.08	0.33

^aIt is noted that the values of $E_{\text{eff,C}_2\text{H}_x}$ denote CH_2CH and C_2H_2 formations on Co_2C (101), (111), and (110) surfaces, respectively, and those of $E_{\text{eff,C}_2\text{H}_x\text{O}}$ denote CHCO formation on Co_2C (101), (110), and (111) surfaces.

Therefore, under realistic FTS conditions, in order to produce more C_{2+} oxygenates on Co_2C catalysts, more Co_2C (111) surface should be exposed, whereas more Co_2C (101) and (110) surfaces should be exposed for C_{2+} hydrocarbon formation, and it has been experimentally confirmed that the preferentially exposed Co_2C (101) surface favors lower olefin production and inhibits CH_4 formation.²² These results illustrate why the previous experimental results for the Co_2C catalyst demonstrated the selectivity toward alcohol synthesis from syngas,^{10,15,17–21} as well as the selectivity toward lower olefin synthesis from syngas.^{22,23} The microscopic reasons point to the crystal facet characteristics of the Co_2C catalyst: namely, the selectivity of C_2 oxygenates and hydrocarbons over the Co_2C catalysts is highly sensitive to the Co_2C crystal facets in the FTS reaction.

3.7. Selectivity between C_2 Oxygenates and Hydrocarbons over $\text{Co}/\text{Co}_2\text{C}$ Catalysts. Experiments by Pei et al.²⁵ found that the Co_2C catalysts used for FTS at 493 K is only partially decomposed into Co , leading to a considerable interface between Co and Co_2C (the $\text{Co}/\text{Co}_2\text{C}$ interface), as confirmed by HRTEM images. Thus, aiming at examining the effect of the Co_2C surface structure and the role of the interface between Co and Co_2C for C_2 oxygenate synthesis, we constructed three simplified and typical structure models on the basis of HRTEM images,²⁵ with a two Co atom wide strip on the Co_2C (101), (110), and (111) surfaces, as shown in Figure 7. The model details are provided in Part 8 in the Supporting Information. These three $\text{Co}/\text{Co}_2\text{C}$ catalyst models correspond to different interfaces due to different Co_2C surfaces. Further, since the CH species is the most favored monomer on the Co_2C (111) and (101) surfaces, both CH and CH_2 species are the most favored monomers on the Co_2C (110) surface, and CO insertion into CH_x ($x = 1, 2$) species is examined on the $\text{Co}/\text{Co}_2\text{C}$ (101), (110), and (111) interface catalysts.

As shown in Figure 8a for the $\text{Co}/\text{Co}_2\text{C}$ (111) interface catalyst, the results show that CO prefers to adsorb at the Co metal part of the Co and Co_2C interface and the CH_x ($x = 1, 2$) intermediate prefers to adsorb at the Co strip, while the adsorbed CO can easily insert into CH_x ($x = 1, 2$) to form C_2 oxygenates CH_xCO with free energy barriers of 0.47 and 0.61 eV, respectively. They are lower by 0.50 and 0.58 eV than those on the pure Co_2C (111). The low free energy barriers for CO insertion into CH_x ($x = 1, 2$) to C_2 oxygenates mean that the $\text{Co}/\text{Co}_2\text{C}$ (111) interface catalyst is indeed favorable for high alcohol formation in comparison to the pure Co_2C (111) surface.

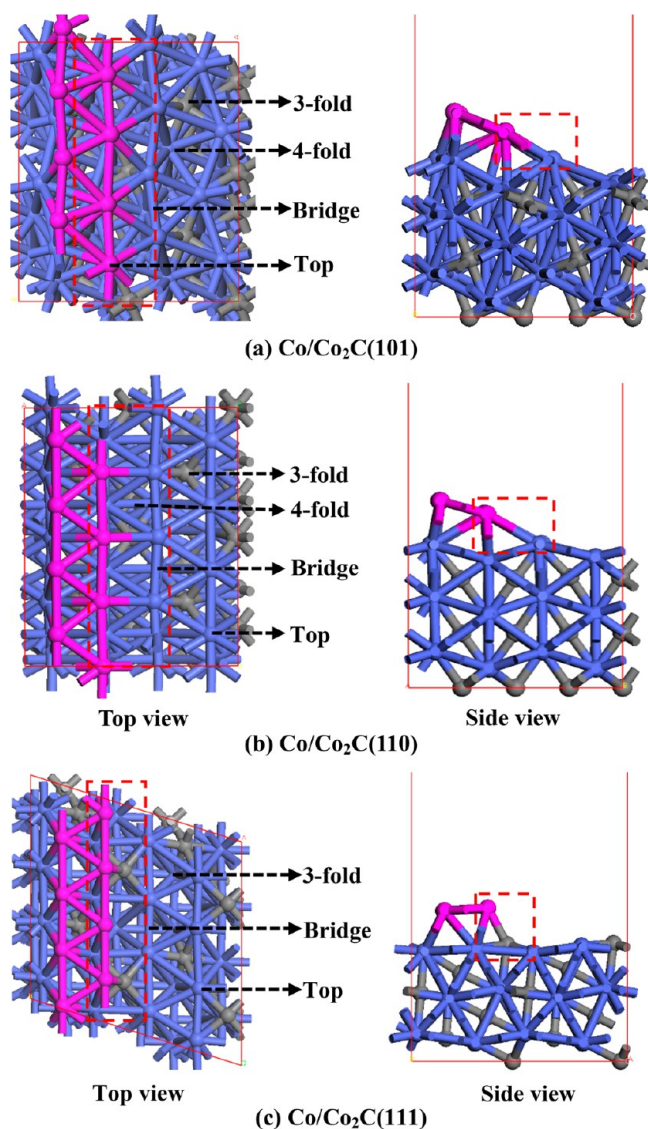


Figure 7. Interface morphology and the corresponding adsorption sites of (a) Co/Co₂C (101), (b) Co/Co₂C (110), and (c) Co/Co₂C (111) interface catalysts. The interface between the Co atom strip and the Co₂C surface is displayed by the red dotted line. Color scheme: rose balls, Co atoms of Co₂C surface; blue balls, Co atoms of metal Co; gray balls, C atoms.

On the Co/Co₂C (110) (see Figure 8b) and Co/Co₂C (101) (see Figure 8c) interface catalysts, CO prefers to adsorb on the Co₂C surface, and the CH_{*x*} (*x* = 1, 2) intermediate prefers to adsorb at the interface between Co and Co₂C. However, the adsorbed CO insertions into CH_{*x*} (*x* = 1, 2) to form C₂ oxygenates CH_{*x*}CO have higher free energy barriers than those on the pure Co₂C (110) and (101) surfaces, suggesting that the Co/Co₂C (110) and Co/Co₂C (101) interface catalysts are not very effective for alcohol formation in comparison to the pure Co₂C (110) and (101) surfaces.

As mentioned above, for C₂ oxygenate formation on the Co/Co₂C interface catalyst, the selectivity between C₂ oxygenates and hydrocarbons still strongly depends on the Co₂C crystal facets. The Co/Co₂C catalyst with Co₂C (111) crystal facet favors C₂ oxygenate formation, whereas the Co/Co₂C catalysts with Co₂C (101) and (110) crystal facets do not favor C₂ oxygenate formation.

According to our projected density of states (PDOS) for the Co/Co₂C (101), Co/Co₂C (110), and Co/Co₂C (111) interface catalysts, as shown in Figure 6b, the d-band center of the Co/Co₂C (111) surface is -1.56 eV, which is higher than that (-1.59 eV) observed on a pure Co₂C (111) surface. For the CO insertion into CH_{*x*} reaction, when the CH_{*x*} fragment interacts with CO and the C–C bond is formed, the doubly occupied 5σ CO orbital interacts with the doubly occupied σ -CH_{*x*} orbital, resulting in doubly occupied bonding and antibonding orbitals, giving a repulsive interaction. The upshift of surface d-band center on the Co/Co₂C (111) catalyst empties more antibonding states,^{29,57} which can accept electrons from the CO and CH_{*x*} fragment orbital in comparison to the pure Co₂C (110) surface and reduce the repulsion, as well as make CO insertion into CH_{*x*} reaction easier, which is also consistent with our kinetics results. However, in comparison to the pure Co₂C (101) and (110) surfaces, the downshift of d-band center on the Co/Co₂C (101) and Co/Co₂C (110) surfaces empties fewer antibonding states, of which only a few accept electrons from the CO and CH_{*x*} fragment orbital and thus inhibit the CO insertion into CH_{*x*}.

The plotted charge density difference of the Co atoms for the Co/Co₂C interface catalyst shown in Figure 9 suggests that the electron densities over the interface of the Co/Co₂C (101) and Co/Co₂C (110) catalysts are greatly reduced, whereas the Co strip and Co₂C (101), and Co₂C (110) surfaces formed electron-rich regions. However, the electron-rich interface of the Co/Co₂C (111) catalyst is formed due to delocalized electron transfer from Co to Co₂C, which greatly facilitates the adsorption and activation of CO and CO insertion into CH_{*x*} (*x* = 1, 2) to form C₂ oxygenates at the Co/Co₂C (111) interface. Indeed, the delocalized electron transfer from the Co atoms to the Co/Co₂C (111) interface is also confirmed by Bader charge analysis. Thus, the electronic effects of the Co/Co₂C (111) binary catalyst result in an increased selectivity toward C₂ oxygenates in comparison to the Co/Co₂C (101) and Co/Co₂C (110) catalysts.

3.8. General Discussion. Overall, the Co₂C (111) surface in both Co₂C and Co/Co₂C catalysts exhibits a higher selectivity toward C₂ oxygenate formation; moreover, the overall contribution to C₂ oxygenate formation focuses on the Co/Co₂C (111) interface catalyst in comparison to the pure Co₂C (111) surface, which confirms the experimental results²⁵ that the high alcohols can be formed at the interface between Co and Co₂C. On the other hand, the Co₂C (110) and (101) surfaces in both Co₂C and Co/Co₂C interface catalysts exhibit a higher selectivity toward C₂ hydrocarbon formation.

Controlling the Co₂C crystal facets can tune the FTS selectivity: namely, one could resort to catalyst morphology control by exposing a large number of active surfaces, which inspires new ways of preparing highly selective Co₂C catalysts: e.g., Watt et al.⁶¹ suggested the uniquely faceted yet stable HCP Ru nanocrystals with a well-defined hourglass shape, exposing exclusively the (10–11) surface, which hints at a desirable Co₂C surface.

The experiment by Pei et al.²⁵ confirmed that, by adding promoters such as La and Zr individually or simultaneously into the Co–Co₂C/AC catalysts, the relative ratio of Co₂C and Co can be controlled. The synthesis of higher alcohols on CaO-promoted Co/AC catalysts²¹ also shows that the relative Co₂C/Co ratio can be controlled via the promoter Ca loading, and a moderate relative Co₂C/Co ratio was found to be favorable for synthesis of mixed C₁–C₁₆ mixed alcohols. Ding

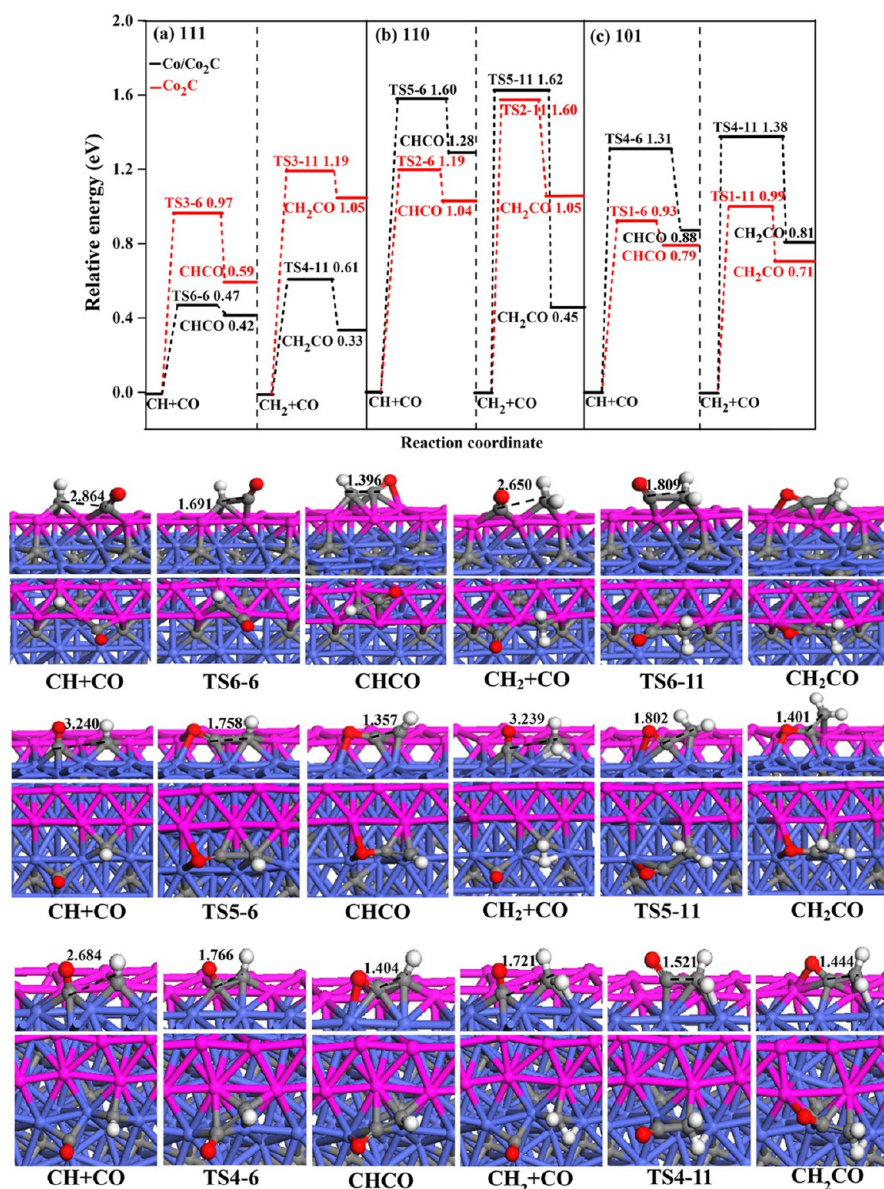


Figure 8. Potential energy profile of CO insertion into CH_x ($x = 1, 2$) to $\text{C}_2\text{H}_x\text{O}$ oxygenates together with the corresponding structures on $\text{Co}/\text{Co}_2\text{C}$ interface catalysts: (a) Co_2C (111) and $\text{Co}/\text{Co}_2\text{C}$ (111); (b) Co_2C (110) and $\text{Co}/\text{Co}_2\text{C}$ (110); (c) Co_2C (101) and $\text{Co}/\text{Co}_2\text{C}$ (101).

and co-workers¹⁰ showed that mixed linear α -alcohols (C_1 – C_{18}) from syngas could be attributed to the high dispersion of Co and the moderate $\text{Co}_2\text{C}/\text{Co}$ ratio over La-doped Co catalysts, which is in accordance with the research of Wang et al.²⁴ Therefore, when the FTS reaction is performed, Co_2C formation and stability and a moderate $\text{Co}_2\text{C}/\text{Co}$ ratio are essential conditions for the synthesis of higher alcohols over Co_2C catalyst. In order to promote Co_2C formation, enhance its stability, obtain a moderate $\text{Co}_2\text{C}/\text{Co}$ ratio, and achieve the optimum selectivity/activity, the Co_2C catalyst has to get help from the promoters, which will be considered in our next work.

Finally, given that the real Co_2C catalyst consists of different crystal facets, probing into the C–C chain formation mechanism on different Co_2C crystal facets can help us gain a better understanding and thus inspire a catalyst design method for the most desirable FTS products. All in all, there is plenty of room for new research to understand the FTS mechanism on different Co_2C surfaces that allow optimizing the FTS product distribution. As of now, we still do not

understand the relationship between the FTS selectivity and the Co_2C catalyst surface for other Co_2C surfaces, such as the Co_2C (011), (010), and (001) surfaces, which is the subject of our current and future work.

4. CONCLUSIONS

In this study, aiming at illustrating the effect of catalyst crystal facets on the selectivity of the C_2 oxygenate and hydrocarbon formation in Fischer–Tropsch synthesis, we have examined the formation mechanism of C_2 oxygenates and hydrocarbons on Co_2C and $\text{Co}/\text{Co}_2\text{C}$ catalysts using density functional theory (DFT) calculations. Three representative low-index Co_2C (101), (110), and (111) surfaces are modeled examples of different Co_2C surface structures. Since CH_x ($x = 1$ – 3), CO, and H species are the key intermediates critical to C_2 oxygenate selectivity, all Fischer–Tropsch reactions related to CH_x ($x = 1$ – 3) species, including CO insertion into CH_x ($x = 1$ – 3) and $\text{CH}_x + \text{CH}_y$ ($x, y = 1$ – 3) coupling to form C_2 species (C_2H_x and $\text{C}_2\text{H}_x\text{O}$), as well as the hydrogenation and dissociation of CH_x

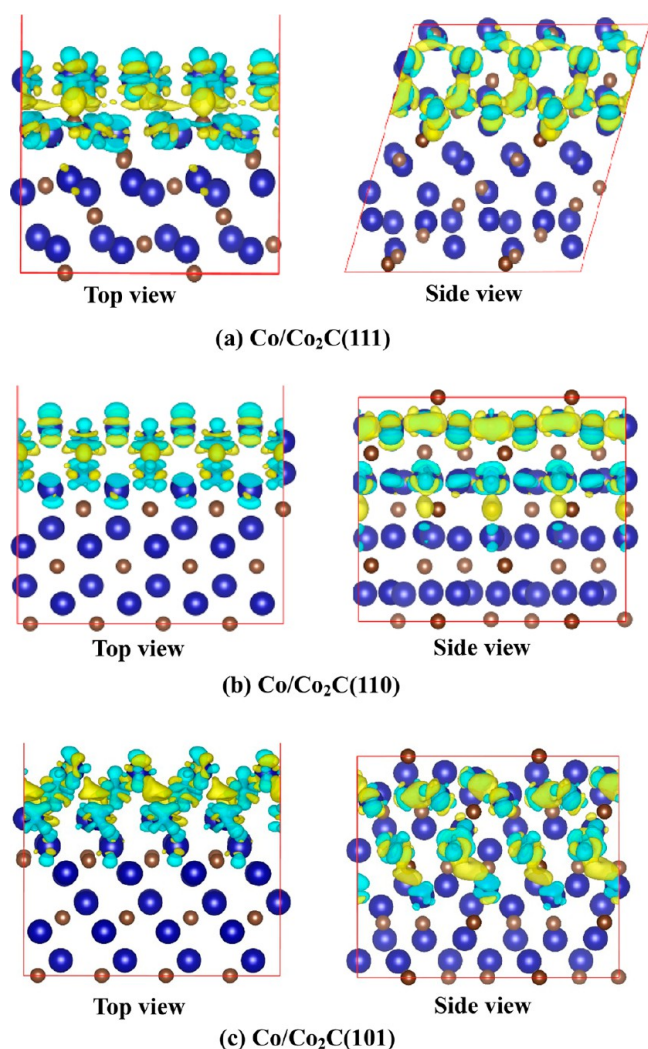


Figure 9. Surface Co charge density differences of Co/Co₂C (111), Co/Co₂C (110), and Co/Co₂C (101) interface catalysts. Green and yellow represent charge depletion and accumulation, respectively.

($x = 1-3$) to form C₁ species (CH₄ and C), are used as examples examined at a FTS temperature at 493 K.

The C₂ species, rather than C₁ species, prefers to be formed on the Co₂C surfaces in FTS. Moreover, the C₂ selectivity, quantitatively estimated from the effective barrier difference, is sensitive to Co₂C surface structure. A Co/Co₂C (111) interface catalyst is more favorable for C₂ oxygenate formation in comparison to the pure Co₂C (111) surface, whereas the Co/Co₂C (110) and Co/Co₂C (101) interface catalysts are unfavorable for C₂ oxygenate formation in comparison to the pure Co₂C (110) and (101) surfaces.

For the FTS over Co₂C and Co/Co₂C catalysts, the Co₂C (111) surface has an unexpectedly high selectivity toward C₂ oxygenates, whereas the Co₂C (101) and (110) surfaces have a high selectivity toward C₂ hydrocarbons. Thus, controlling the crystal facets of Co₂C catalysts using well-defined preparation methods is an effective tool to tune the FTS selectivity toward the most desirable products.

■ ASSOCIATED CONTENT

Supporting Information

The Supporting Information is available free of charge on the ACS Publications website at DOI: 10.1021/acscatal.7b02800.

Descriptions of the Co₂C surface, methods for calculating the Gibbs free energy, rate constants and effective barriers, the most stable adsorption configurations of all adsorbed species, the reactions related to CH_x ($x = 1-3$) species, and the Co/Co₂C (111) interface model construction (PDF)

■ AUTHOR INFORMATION

Corresponding Authors

*E-mail for B.W.: wangbaojun@tyut.edu.cn.

*E-mail for M.F.: mfan@uwyo.edu.

ORCID

Maohong Fan: 0000-0003-1334-7292

Notes

The authors declare no competing financial interest.

■ ACKNOWLEDGMENTS

This work was financially supported by the National Natural Science Foundation of China (No. 21476155, 21776193, 21736007), the China Scholarship Council (201606935026), the Program for the Top Young Academic Leaders of Higher Learning Institutions of Shanxi, the Top Young Innovative Talents of Shanxi, and the U.S. NSF-sponsored NCAR-Wyoming Supercomputing Center (NWS-C).

■ REFERENCES

- (1) Geerlings, J. J. C.; Wilson, J. H.; Kramer, G. J.; Kuipers, H. P. C. E.; Hoek, A.; Huisman, H. M. *Appl. Catal., A* **1999**, *186*, 27–40.
- (2) Huo, C. F.; Li, Y. W.; Wang, J. G.; Jiao, H. J. *J. Phys. Chem. C* **2008**, *112*, 14108–14116.
- (3) Cheng, J.; Hu, P.; Ellis, P.; French, S.; Kelly, G.; Lok, C. M. *J. Phys. Chem. C* **2008**, *112*, 9464–9473.
- (4) Ojeda, M.; Nabar, R.; Nilekar, U. A.; Ishikawa, A.; Mavrikakis, M.; Iglesia, E. *J. Catal.* **2010**, *272*, 287–297.
- (5) Ciobica, I. M.; Santen, R. A. V. *J. Phys. Chem. B* **2003**, *107*, 3808–3812.
- (6) Haider, M. A.; Gogate, M. R.; Davis, R. J. *J. Catal.* **2009**, *261*, 9–16.
- (7) Remediakis, I. N.; Abild-Pedersen, F.; Nørskov, J. K. *J. Phys. Chem. B* **2004**, *108*, 14535–14540.
- (8) Cheng, J.; Hu, P.; Ellis, P.; French, S.; Kelly, G.; Lok, C. M. *Top. Catal.* **2010**, *53*, 326–337.
- (9) Dong, W.; Liu, J.; Zhu, H.; Ding, Y.; Pei, Y.; Liu, J.; Du, H.; Jiang, M.; Liu, T.; Su, H.; Li, W. *J. Phys. Chem. C* **2014**, *118*, 19114–19122.
- (10) Jiao, G.; Ding, Y.; Zhu, H.; Li, X.; Li, J.; Lin, R.; Dong, W.; Gong, L.; Pei, Y.; Lu, Y. *Appl. Catal., A* **2009**, *364*, 137–142.
- (11) Zhao, Y. H.; Su, H. Y.; Sun, K.; Liu, J. X.; Li, W. X. *Surf. Sci.* **2012**, *606*, 598–604.
- (12) Bian, G. Z.; Nanba, T.; Koizumi, N.; Yamada, M. *J. Mol. Catal. A: Chem.* **2002**, *178*, 219–228.
- (13) Weller, B. Y.; Hofer, L. J. E.; Anderson, R. B. *J. Am. Chem. Soc.* **1948**, *70*, 799–801.
- (14) Xiong, J. M.; Ding, Y. J.; Wang, T.; Yan, L.; Chen, W. M.; Zhu, H. J.; Lu, Y. *Catal. Lett.* **2005**, *102*, 265–269.
- (15) Volkova, G. G.; Yurieva, T. M.; Plyasova, L. M.; Naumova, M. I.; Zaikovskii, V. I. *J. Mol. Catal. A: Chem.* **2000**, *158*, 389–393.
- (16) Xiang, Y. Z.; Kruse, N. *Nat. Commun.* **2016**, *7*, 13058.
- (17) Fang, Y. Z.; Liu, Y.; Zhang, L. H. *Appl. Catal., A* **2011**, *397*, 183–191.
- (18) Fang, Y. Z.; Liu, Y.; Deng, W.; Liu, J. H. *J. Energy Chem.* **2014**, *23*, 527–534.
- (19) Pei, Y. P.; Ding, Y. J.; Zhu, H. J.; Zang, J.; Song, X. G.; Dong, W. D.; Wang, T.; Yan, L.; Lu, Y. *React. Kinet., Mech. Catal.* **2014**, *111*, 505–520.

- (20) Pei, Y. P.; Ding, Y. J.; Zang, J.; Song, X. G.; Dong, W. D.; Zhu, H. J.; Wang, T.; Chen, W. M. *Chin. J. Catal.* **2015**, *36*, 252–259.
- (21) Du, H.; Zhu, H. J.; Chen, X. K.; Dong, W. D.; Lu, W.; Luo, W. T.; Jiang, M.; Liu, T.; Ding, Y. J. *Fuel* **2016**, *182*, 42–49.
- (22) Zhong, L. S.; Yu, F.; An, Y. L.; Zhao, Y. H.; Sun, Y. H.; Li, Z. J.; Lin, T. J.; Lin, Y. J.; Qi, X. Z.; Dai, Y. Y.; Gu, L.; Hu, J. S.; Jin, S. F.; Shen, Q.; Wang, H. *Nature* **2016**, *538*, 84–87.
- (23) Li, Z. J.; Zhong, L. S.; Yu, F.; An, Y. L.; Dai, Y. Y.; Yang, Y. Z.; Lin, T. J.; Li, S. G.; Hui Wang, H.; Gao, P.; Sun, Y. H.; He, M. Y. *ACS Catal.* **2017**, *7*, 3622–3631.
- (24) Lebarbier, V. M.; Mei, D. H.; Kim, D. H.; Andersen, A.; Male, J. L.; Holladay, J. E.; Rousseau, R.; Wang, Y. J. *Phys. Chem. C* **2011**, *115*, 17440–51.
- (25) Pei, Y. P.; Liu, J. X.; Zhao, Y. H.; Ding, Y. J.; Liu, T.; Dong, W. D.; Zhu, H. J.; Su, H. Y.; Yan, L.; Li, J. L.; Li, W. X. *ACS Catal.* **2015**, *5*, 3620–3624.
- (26) Mohandas, J. C.; Gnanamani, M. K.; Jacobs, G.; Ma, W.; Ji, Y.; Khalid, S.; Davis, B. H. *ACS Catal.* **2011**, *1*, 1581–1588.
- (27) Zhang, R. G.; Wang, G. R.; Wang, B. J. *J. Catal.* **2013**, *305*, 238–255.
- (28) Zhao, Y. H.; Sun, K. J.; Ma, X. F.; Liu, J. X.; Sun, D. P.; Su, H. Y.; Li, W. X. *Angew. Chem., Int. Ed.* **2011**, *50*, 5335–5338.
- (29) Choi, Y. M.; Liu, P. J. *Am. Chem. Soc.* **2009**, *131*, 13054–13061.
- (30) Pan, Y. X.; Liu, C. J.; Ge, Q. F. *J. Catal.* **2010**, *272*, 227–234.
- (31) Chin, Y. H.; Buda, C.; Neurock, M.; Iglesia, E. *J. Catal.* **2011**, *283*, 10–24.
- (32) U.S. Bureau of Mines. *Bulletin 578*; U.S. Government Print Office: Washington, DC, 1948–1959; <http://www.fischer-tropsch.org>.
- (33) Huo, C. F.; Li, Y. W.; Wang, J. G.; Jiao, H. J. *J. Am. Chem. Soc.* **2009**, *131*, 14713–14721.
- (34) Pham, T. H.; Qi, Y. Y.; Yang, J.; Duan, X. Z.; Qian, G.; Zhou, X. G.; Chen, D.; Yuan, W. K. *ACS Catal.* **2015**, *5*, 2203–2208.
- (35) Kresse, G. *Phys. Rev. B: Condens. Matter Mater. Phys.* **1993**, *47*, 558–561.
- (36) Kresse, G.; Hafner, J. *Phys. Rev. B: Condens. Matter Mater. Phys.* **1994**, *49*, 14251–14269.
- (37) Kresse, G.; Furthmüller, J. *Phys. Rev. B: Condens. Matter Mater. Phys.* **1996**, *54*, 11169–11186.
- (38) Blöchl, P. E. *Phys. Rev. B: Condens. Matter Mater. Phys.* **1994**, *50*, 17953–17979.
- (39) Kresse, G.; Joubert, D. *Phys. Rev. B: Condens. Matter Mater. Phys.* **1999**, *59*, 1758–1775.
- (40) Zhuo, M.; Tan, K. F.; Borgna, A.; Saeys, M. J. *Phys. Chem. C* **2009**, *113*, 8357–8365.
- (41) Perdew, J. P.; Chevary, J. A.; Vosko, S. H.; Jackson, K. A.; Pederson, M. R.; Singh, D. J.; Fiolhais, C. *Phys. Rev. B: Condens. Matter Mater. Phys.* **1993**, *48*, 4978–4978.
- (42) Wang, Y.; Perdew, J. P. *Phys. Rev. B: Condens. Matter Mater. Phys.* **1991**, *44*, 13298–13307.
- (43) Monkhorst, H. J.; Pack, J. D. *Phys. Rev. B* **1976**, *13*, 5188–5192.
- (44) Henkelman, G.; Uberuaga, B. P.; Jónsson, H. *J. Chem. Phys.* **2000**, *113*, 9901–9904.
- (45) Henkelman, G.; Jónsson, H. *J. Chem. Phys.* **2000**, *113*, 9978–9985.
- (46) Henkelman, G.; Jónsson, H. *J. Chem. Phys.* **1999**, *111*, 7010–7022.
- (47) Sun, K. j.; Zhao, Y. H.; Su, H. Y.; Li, W. X. *Theor. Chem. Acc.* **2012**, *131*, 1–10.
- (48) Khodakov, A. Y. *Catal. Today* **2009**, *144*, 251–257.
- (49) Pan, W. X.; Cao, R.; Griffin, G. L. *J. Catal.* **1988**, *114*, 447–456.
- (50) Cheng, J.; Gong, X. Q.; Hu, P.; Lok, C. M.; Ellis, P.; French, S. J. *Catal.* **2008**, *254*, 285–295.
- (51) Zhuo, M. K.; Borgna, A.; Saeys, M. J. *Catal.* **2013**, *297*, 217–226.
- (52) Clay, J. P.; Greeley, J. P.; Ribeiro, F. H.; Delgass, W. N.; Schneider, W. F. *J. Catal.* **2014**, *320*, 106–117.
- (53) Cao, X. M.; Burch, R.; Hardacre, C.; Hu, P. *Catal. Today* **2011**, *165*, 71–79.
- (54) Liu, J. X.; Su, H. Y.; Sun, D. P.; Zhang, B. Y.; Li, W. X. *J. Am. Chem. Soc.* **2013**, *135*, 16284–16287.
- (55) Ge, Q.; Neurock, M.; Wright, H. A.; Srinivasan, N. *J. Phys. Chem. B* **2002**, *106*, 2826–2829.
- (56) Zhang, R. G.; Liu, F.; Wang, Q.; Wang, B. J.; Li, D. B. *Appl. Catal. A: Gen.* **2016**, *186*, 3–12.
- (57) Li, J. D.; Croiset, E.; Luis, R. S. *J. Mol. Catal. A: Chem.* **2012**, *365*, 103–114.
- (58) Storsæter, S.; Chen, D.; Holmen, A. *Surf. Sci.* **2006**, *600*, 2051–2063.
- (59) Cheng, J.; Hu, P.; Ellis, P.; French, S.; Kelly, G.; Lok, C. M. *J. Phys. Chem. C* **2008**, *112*, 6082–6086.
- (60) Cheng, J.; Hu, P.; Ellis, P.; Kelly, G.; Lok, C. M. *J. Phys. Chem. C* **2009**, *113*, 8858–8863.
- (61) Watt, J.; Yu, C.; Chang, S. L. Y.; Cheong, S.; Tilley, R. D. *J. Am. Chem. Soc.* **2013**, *135*, 606–609.